RSC Advances

PAPER

View Article Online
View Journal | View Issue

Cite this: *RSC Adv.*, 2018, **8**, 20477

Quantum confined two-dimensional electron/hole gas switching by facet orientation of perovskite oxides†

Fei Zhou,[ab] Yong Liu,[ad] Zhonghong Lai,[e] Mingqing Liao,[a] Yi Zhou,[a] Yudong Huang[b] and Jingchuan Zhu*[acd]

Received 8th May 2018
Accepted 29th May 2018

DOI: 10.1039/c8ra03928c

rsc.li/rsc-advances

The Polar discontinuity at heterointerface and the bare surface reconstructs the electronic phase of perovskite oxides. This gives rise to confined free electrons which intrinsically transit material from band insulator to metal. However, the insulator–metal transition induced by free holes has not been investigated so far due to the challenge in obtaining free hole state in oxides. Here, we propose a simple method whereby free holes can be obtained *via* polar facet reorientation. In the high polarity case, free holes can be supported by the lift up of O 2p subbands, which split into three independent subbands (one heavy hole subband and two light hole subbands) due to strong quantum confinement. Results show that both of the free electron and hole states are confined in a two dimensional quantum well, subjecting to the confined energy ($E - E_F$) and occupied density of states around the Fermi level, indicating a finite thickness for preserving the metal states.

Introduction

Two-dimensional electron/hole gases (2DEGs/2DHGs) were first studied at the interfaces of semiconductor heterostructures.[1,2] Recent studies have revealed the existence of high mobility 2DEGs at $LaAlO_3/SrTiO_3$ interface[3] and even at the bare surface of $SrTiO_3$,[4,5] which are treated as the cornerstone of oxide electronics.[6] Electronic reconstruction at interfaces or surfaces that occur to compensate for the polar discontinuity of adjacent constituents plays a key role in the formation of localized 2DEGs.[7] This gives rise to attractive physics, such as insulating-metallic state transitions,[8] superconductivity,[9] spiral magnetism and giant negative magnetoresistance.[10–12] These above-mentioned examples occur on n-type interface/surface, such as the interface construction of $(LaO)^+/(TiO_2)^0$ or with defects created on bare $SrTiO_3$ surface, leading to the mixed dimensionality of confined conducting electrons.[13] On the contrary, it is still challenging to obtain the free holes at interfaces or surfaces of oxides,[3,14] although recent experiment shows that strong hole carriers can be seen at the $LaAlO_3/SrTiO_3$ heterointerface by reducing the oxygen defects.[15,16] However, 2DHGs have been researched in Ge/Si based semiconductor heterostructures, presenting novel physics, such as spin Hall effect induced edge-spin accumulation and well-controlled Coulomb blockade oscillations.[17–19] The lack of investigations of 2DHGs on perovskite oxides might be ascribed to the limitation of current epitaxial growth technology, which generally allows films to grow along $(001)_{cubic}$ direction through substrate matching, preserving an extra $e^-/2$ per unit cell on the discontinued interface or surface. Our recent experiments show that 2D potassium niobates can be grown automatically in liquid with facets of 60° tilting of oxygen octahedrons, providing a practical basis for the study of the facets effects to 2DEGs/2DHGs.

In this letter, *ab initio* calculation is used to investigate the confined 2DEGs/2DHGs in 2D $KNbO_3$. Results show that the increase of polar discontinuity by facets engineering would change the electronic phase of the material surface, leading to the formation of switchable 2DEGs and 2DHGs on 2D $KNbO_3$ structures by varying facet orientations. These free electron/hole states around the Fermi level (E_F) are strongly quantum localized. This concept not only endows the material with an

[a]*School of Materials Science and Engineering, Harbin Institute of Technology, 150001, Harbin, China. E-mail: fgms@hit.edu.cn*
[b]*MIIT Key Laboratory of Critical Materials Technology for New Energy Conversion and Storage, School of Chemistry and Chemical Engineering, Harbin Institute of Technology, 150001, Harbin, China*
[c]*National Key Laboratory of Science and Technology on Advanced Composites in Special Environments, Harbin Institute of Technology, 150001, Harbin, China*
[d]*National Key Laboratory for Precision Hot Processing of Metals, Harbin Institute of Technology, 150001, Harbin, China*
[e]*Analysis and Testing Center, Harbin Institute of Technology, 150001, Harbin, China*

† Electronic supplementary information (ESI) available: Computation methods, surface slabs of different facets of $KNbO_3$, band structure of trilayers models of 2D $KNbO_3$, crystal models of $(100)_{orth}$ oriented 2D $KNbO_3$, band structures of $(100)_{orth}$ oriented 2D crystal, states occupation below E_F of $(100)_{orth}$ oriented 2D crystals, free electrons absorptions of $(100)_{orth}$ oriented 2D $KNbO_3$, crystal models of $(120)_{orth}$ oriented 2D crystal, band structures of $(120)_{orth}$ oriented 2D crystal, electronic structures of bulk $KNbO_3$ crystal (PDF). See DOI: 10.1039/c8ra03928c

insulator–metal transition, but also provide an opportunity for manipulating 2DEGs/2DHGs in the quantum confined regime.

Computational details

The first-principle calculation is performed with the Cambridge Serial Total Energy Package.[20] 2D crystal models are fully relaxed through geometry optimization according to system energy, force and stress by DFT with the Perdew, Burke, and Ernzerhof functional.[21] For our main objective is qualitatively investigating the behaviors of quantum confined free electronic states, ultrasoft pseudopotentials are applied to describe the ionic cores with a plane-wave cutoff energy of 340 eV. The *k*-point sampling grids are $3 \times 3 \times 1$ for 2D crystal slabs and $4 \times 4 \times 2$ for bulk $KNbO_3$ crystal, respectively. The vacuum spacing layer between neighboring repeat units of 2D slabs are set to 1 nm. The truncated surface are capped by H atoms, in order to neutralize the surface dangling oxygen bonds.

The surface energy E_s is computed using the formula $E_s = (E_{slab} - nE_{bulk})/2A$,[22] where E_{slab} and E_{bulk} are the total energy of the 2D slab and the bulk per unit cell, respectively. They are all obtained by DFT calculation. n is the number of bulk unit cell contained in the 2D slab. $2A$ is the surface area of each 2D slabs.

Results and discussion

2DEGs/2DHGs switching

$KNbO_3$ is a typical orthorhombic ferroelectric with K^+ and Nb^{5+}, showing different valence discontinuity from conventional $SrTiO_3$ in various facets orientation. In order to know the facets differences of orthorhombic $KNbO_3$, density functional theory is used. Two dimensional (2D) slabs with tilted oxygen octahedrons in angles of 0°, 60°, 90° are built (as sketched in Fig. 1, the 2D slabs used for DFT calculation see Fig. S1†). Calculated results show that the facets of $(100)_{orth}$, $(011)_{orth}$ and $(01\bar{1})_{orth}$ (0° tilting of oxygen octahedron, see Fig. 1a), which are perpendicular to one another with a terminal plane of $(KO)^-$, have small surface energy (E_s) below 100 MeV $Å^{-2}$ (see Table 1). Lower surface energies explains why $KNbO_3$ crystals always grow as cubic particle in hydrostatic reactions. These facets correspond to the $(100)_{cub}$, $(010)_{cub}$ and $(001)_{cub}$ oriented facets in cubic $SrTiO_3$ respectively, but with distinct valence difference in alternate atomic layers, $(SrO)^0/(TiO_2)^0$ in $SrTiO_3$ and $(KO)^-/(NbO_2)^+$ in $KNbO_3$. Besides 0° tilted octahedron 2D models, the E_s of 60° and 90° tilted models (Fig. 1b and c) are all between 150 MeV $Å^{-2}$ and 300 MeV $Å^{-2}$, maintaining a strong energy barrier in self-driven growth processes. The large differences in surface energies will work on the formation of stable surface structures of 2D $KNbO_3$. This further results in their distinct electronic reconstructions on the surface.

To investigate the relevance of surface energy to surface polar properties, trilayers 2D models of $KNbO_3$ crystal with $(100)_{orth}$ and $(120)_{orth}$ facet orientations are built. After lattice relaxation, stable 2D structures are obtained (Fig. 2a and c). Their electronic structures are calculated. Specifically, the 60° tilted facet of $(120)_{orth}$ 2D crystal shows an alternating valence variation of $(KO_3)^{5-}/Nb^{5+}$, indicating a potential huge polar difference in alternating atomic planes, as shown in Fig. 2d. From the sliced mapping of electron localization functions (ELF) in Fig. 2b and d, quantum confined surface states can be clearly observed on both surfaces, which surround the perfectly localized core and the bonding electrons (where ELF approaches 1)[23] of oxygen atoms, allowing the electron and hole carriers moving freely on the surface. In consideration of the distinct electronic reconstructions, $(100)_{orth}$ with extra $e^-/2$ (N-type) and $(120)_{orth}$ with extra $3h^+/2$ (P-type) injection per unit cell, their electronic phases should be different. Fig. 3a and b show the calculated bands around E_F of $(100)_{orth}$ and $(120)_{orth}$ oriented 2D $KNbO_3$. Conventional free electron conductance switches to free hole conductance when a facet of $(100)_{orth}$ changes to $(120)_{orth}$ by the 60° tilting of oxygen octahedrons. The preferential growth facet also changes the symmetry of electronic states transitions, resulting in an indirect optical band gap transition changing to direct at Γ point, as the red arrows indicated in ESI Fig. S2a and S2b.† Density of states of s, p, d orbits (Fig. 3c and d) shows further insights of this switching behavior. The potential of low-lying conduction band descends by 0.39 eV due to extra electron injection, pushing the Nb 4d band to E_F and allowing electrons to move freely at the bottom of the conduction band (Fig. 3c). Conversely, extra holes injection induced by strongly quantized O 2p states lifts the valence band by 0.17 eV above E_F, giving free holes. The low-

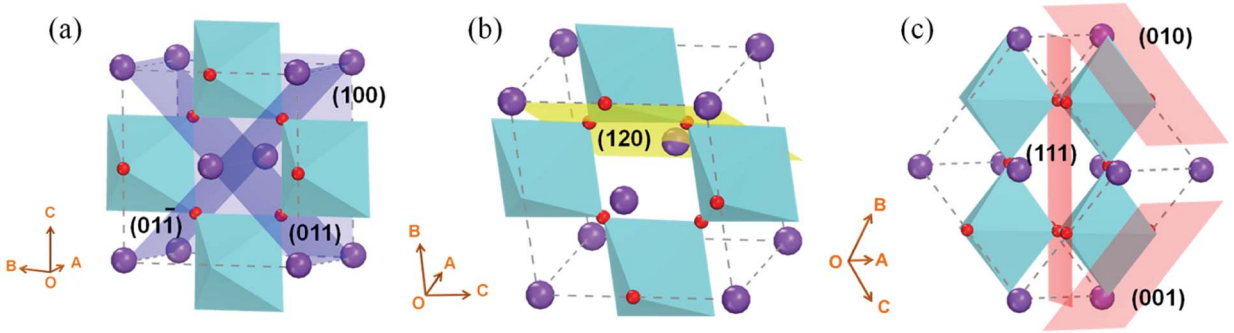

Fig. 1 (a) (100), (011) and (01$\bar{1}$) facets of *Amm*2 orthorhombic $KNbO_3$ (cut plane marked by blue) with 0° tilt of oxygen octahedrons, these three facets are perpendicular to each other, forming a cubic morphology. (b) (120) facet (cut plane marked by yellow) with 60° tilt of oxygen octahedrons, shows a pseudo-hexagonal symmetry in plane. (c) (001), (010) and (111) facets (cut plane marked by red) with 90° tilt of oxygen octahedrons.

Table 1 The energy difference of 2D slab to bulk ($E_{slab} - E_{bulk}$), surface areas (S), surface energy (E_s) of 2D $KNbO_3$ with different facets

	(100)	(011)	(01$\bar{1}$)	(001)	(010)	(111)	(120)
$E_{slab} - E_{bulk}$ (eV)	11.68	4.68	3.34	55.68	40.68	44.68	51.68
Surface (Å^2)	67.446	65.404	65.404	92.224	92.768	140.926	113.338
E_s (eV Å^{-2})	0.086	0.033	0.026	0.298	0.217	0.158	0.227

lying subbands of Nb 4d are split t_{2g} bands, composed of a heavy (d_{yz} doublet) and a light (d_{xy} singlet) band.[24] Strong confinement lifts up the light t_{2g} band with respect to the heavy ones (Fig. 3a), demonstrated in the thickness dependence of band structures variations of $(100)_{orth}$ models (See Fig. S4†), due to the difference in m_e. The top O 2p bands also split into three subbands, the highest heavy (E_{hb}^+) and underlying two light (E_{lb}^+) ones (Fig. 3b) under the quantum confined regime.

Quantized electronic states in a 2D square quantum well

To obtain the effect of the size limitation to free electronic states, the band structures of $(120)_{orth}$ 2D $KNbO_3$ with thicknesses that range from 0.23 nm (1 octahedron layer) to 4.6 nm (20 octahedron layers) are calculated (see Fig. S8†). Strong quantum confinement can be observed with a decrease in thickness, accompanied by the splitting of degenerate energy into independent sub-bands, as indicated by the red arrow in ESI Fig. S8.† A two-dimensional square quantum well is used to describe the thickness dependence of quantum confined band gaps, given by: $E_g = E_g^0 + \frac{\hbar^2\pi^2}{2m^*r^2}$,[25] where E_g is the calculated energy gap of the 2D model and E_g^0 is the calculated energy gap of the bulk crystal model ($E_g^0 \sim 2.3$ eV, as shown in ESI Fig. S9†). The second term represents quantum localization, where $\hbar$ is the reduced Planck's constant, r is the sheet thickness, and $m^* = \left(\frac{1}{m_e} + \frac{1}{m_h}\right)^{-1}$ is the reduced effective mass. Fig. 4a plots the calculated thickness dependence of quantum well transition energies with dimension reduction. The value of m^* is 0.6 m_e, which is obtained from fitting a best fit line to calculate E_g values (pink dotted line in Fig. 4a). The solid fit line in the inset confirms the linear relationship of quantum confined energies to $1/r^2$ for a 2D square quantum well.

The hole states occupation of samples are shown in Fig. 4b–h. A monotonous decreasing relationship of confined energy of hole states with respect to the thicknesses of 2D wells is observed, where the O 2p bands will be totally under E_F when thickness approaches 4.6 nm. Strong confinement leads to the splitting of the top O 2p band into one heavy (E_{hb}^+, denoted as red dots) and two light (E_{lb1}^+ and E_{lb2}^+, denoted as blue and green dots respectively) bands at Γ point. The decrease in quantum confined energy contributes to the appearance of degenerate E_{hb}^+ and E_{lb1}^+ bands (as shown in Fig. 4b–f), accompanied by the gradual increase of m_h of E_{lb1}^+ along momentum k. Until reaching the weak confined situation (Fig. 4g), the light E_{lb2}^+ band descends down to E_F first, then degenerate E_{hb}^+ and E_{lb1}^+ bands will further combine with E_{lb2}^+ and totally descend under E_F (Fig. 4h). A similar trend of low-lying conduction t_{2g} band of $(100)_{orth}$ models being lifted up to E_F can be observed with an increase in thickness (see ESI

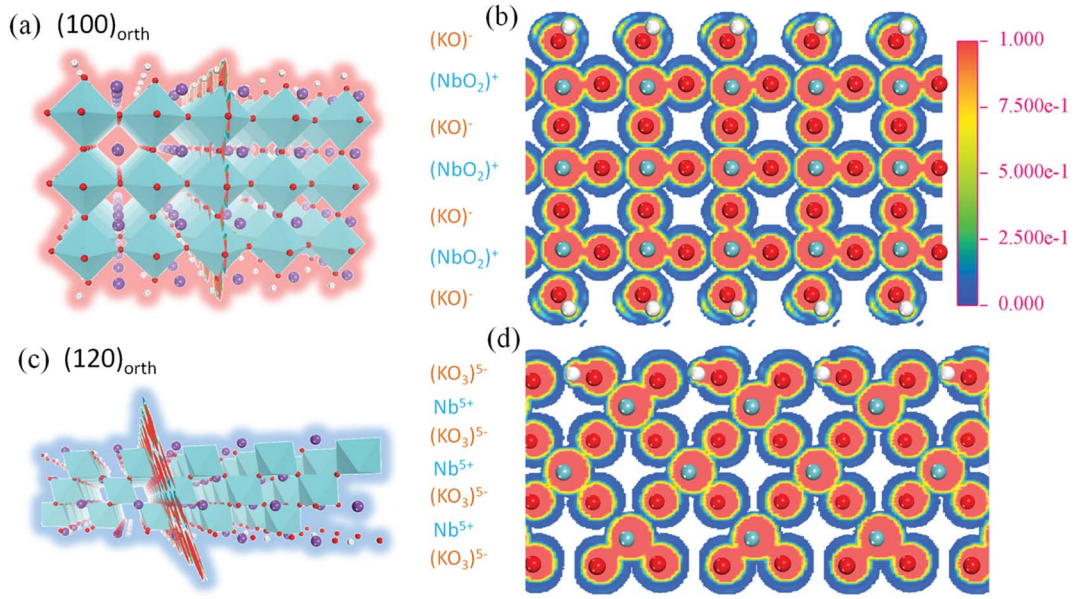

Fig. 2 (a) and (c) The trilayers (octahedron layer) atomic structures of $(100)_{orth}$ and $(120)_{orth}$ oriented 2D $KNbO_3$ models, surface dangling bonds of oxygen were capped by hydrogen atoms, the selected cutting slices of Nb–O plane of calculated ELF in (a) and (c) were showed in (b) and (d) by colored maps, respectively. Both of the 2D structures were obtained by energy minimization through optimizing geometry.

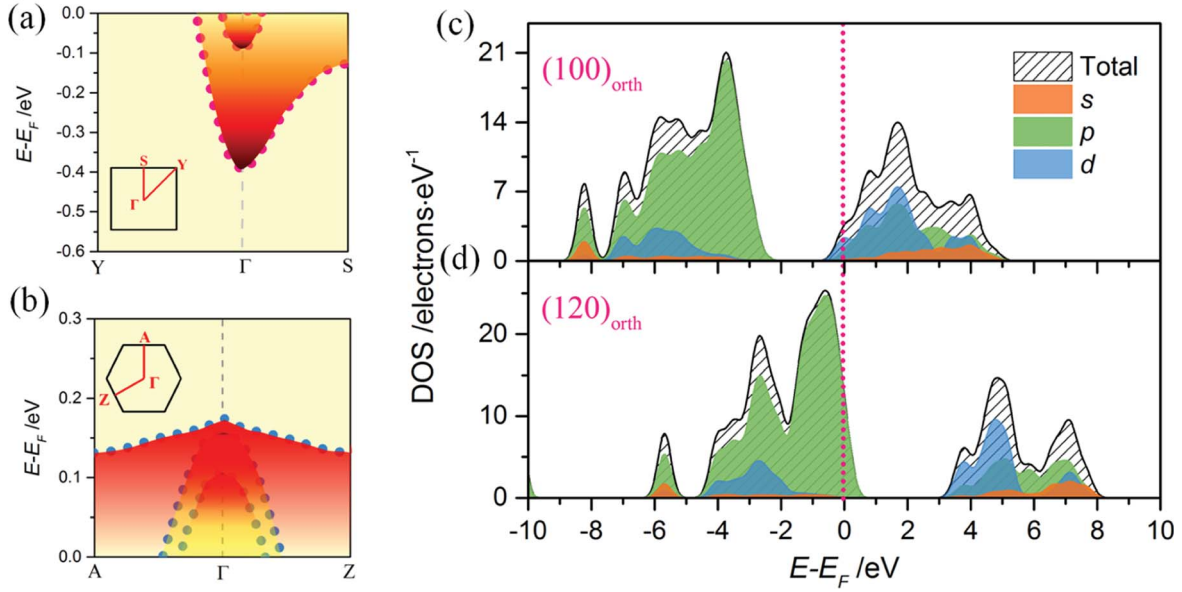

Fig. 3 (a) and (b) Calculated band structures of trilayers (octahedron layer) $(100)_{orth}$ and $(120)_{orth}$ oriented 2D $KNbO_3$ models, respectively. Free electron states switch to free holes when facets changed. (c) and (d) Partial density of states of s, p, d orbits of both of 2D $KNbO_3$ models, respectively. Oblique fill lines show the sum of DOS of different orbits.

Fig. S5†), showing that both of 2DEG and 2DHG cases have strong quantum confinement along the *Z* direction.

Insulator–metal transition

To obtain further insight of the insulator–metal transition of our 2DFEG/2DFHG systems, optical absorption properties of models with varying thicknesses are calculated. Fig. 5a shows the absorption spectra of $(120)_{orth}$ oriented 2D $KNbO_3$ models (thicknesses are from 0.46 nm to 4.6 nm). The strong absorption across the whole optical gap demonstrates the insulator–metal transition. Fig. 5b plots the maximum absorption of the free hole states (collected from low-frequency absorption spectra, as shown in inset figure), showing that the free holes absorption intensity increase gradually with an increase in thickness. Up to above 1.15 nm (5 layers), it decreased dramatically with an increase in thickness, indicating a critical thickness of about 2 nm for the existence of metallic states for 2DHGs. A gradual blue-shift of intrinsic absorption band edges can be observed when the number of layers increases (indicated by the blue arrow in Fig. 5a), along with one single peak extending to two individual peaks (as pink arrow indicated in Fig. 5a) due to the splitting and lifting of s, p orbits from the

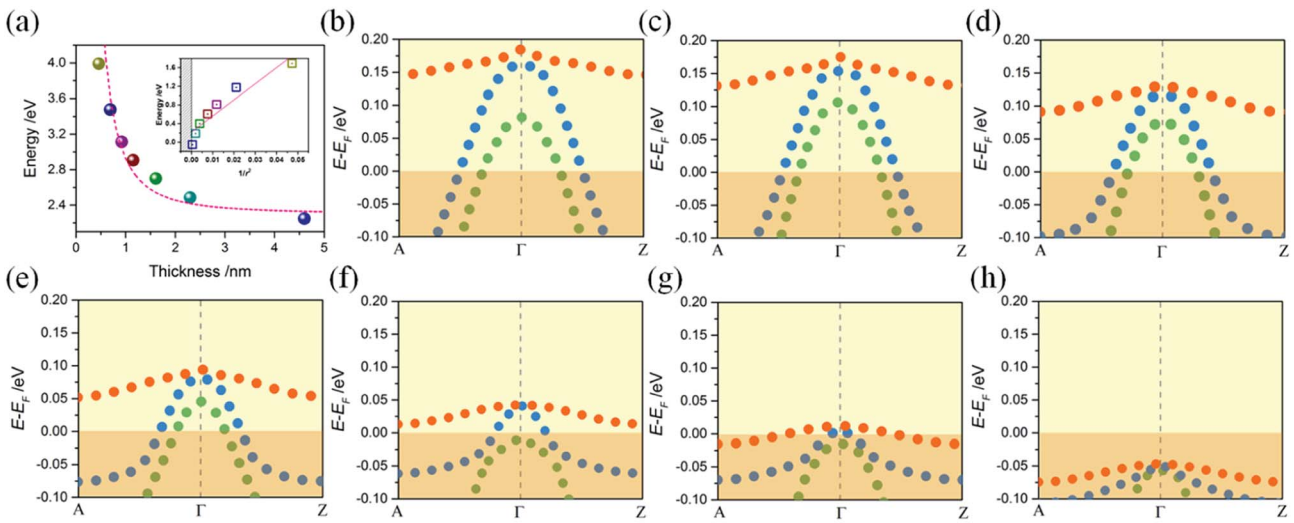

Fig. 4 (a) Colored balls correspond to the calculated band gap energy of 2D models with thicknesses varying from 0.46 nm to 4.6 nm. The abrupt increase in band gap energy occurs at below 2 nanometer size, where there is a presence of strong quantum confinement. The theoretically calculated curve (pink dotted line) fits very well to the experimental data. Inset illustrates the linear relationship between the quantum confinement effected energy values and $1/r_2$. (b)–(h) The evolution of quantum localized hole states with 2D well thickness varying. Red dotted line denotes the heavy hole (E_{hb}^{+}) band, blue and green dotted lines denote the two light (E_{lb1}^{+} and E_{lb2}^{+}) bands.

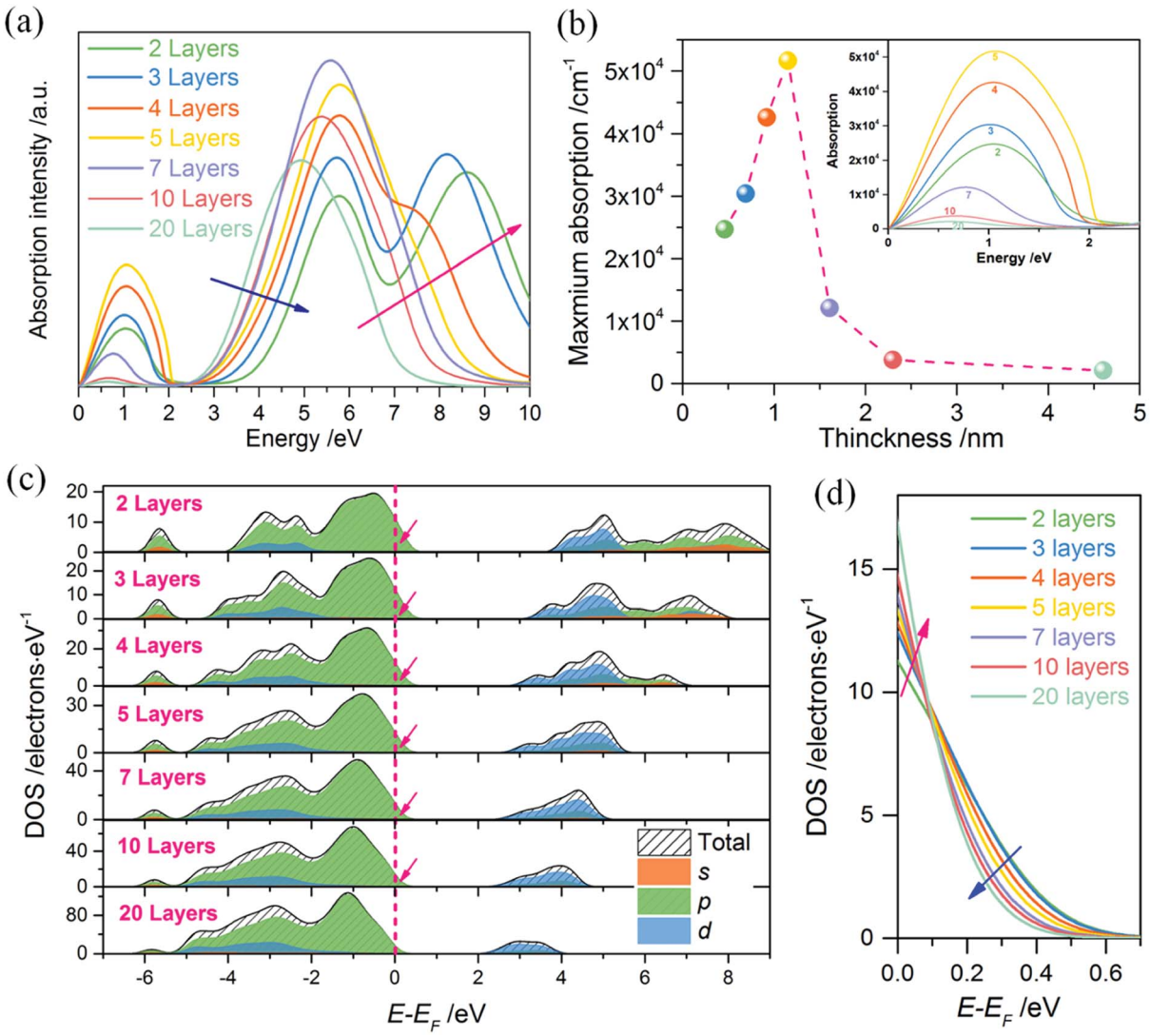

Fig. 5 (a) Absorption properties of $(120)_{orth}$ oriented 2D $KNbO_3$ models, the absorption in low frequency indicates an insulator–metal transition absorption. (b) The thickness dependences of absolute absorption intensity of free hole states, inset is the zoom in of low-frequency range. (c) PDOS of $(120)_{orth}$ oriented 2D $KNbO_3$ with thickness range from 2 layers to 20 layers, show the thickness dependence of quantum localized free holes and the corresponding contributions of different orbits. (d) Evolution trend of quantized hole states with respect to the thickness varying. The quantum localized energy and the absolute value of electronic states per electron volt co-work on the free hole states absorption, showing a converse contribution (as the blue and pink arrows indicating with reverse directions).

degenerate d band (Fig. 5c). This agrees with the quantized characters of conduction band in 2D quantum well. Although the occupation energy of hole states above E_F decreases with an increase in well thickness (such as the pink arrow marked in Fig. 5c and blue arrow marked in Fig. 5d), the increase of DOS near E_F (marked by pink arrow in Fig. 5d) competes with the decrease of confined energy, leading to an increase initially then decrease of free hole states absorptions. The increase in DOS near E_F is ascribed to the increased total numbers of atoms per unit area when stacking layers increase. However, the confined energy still plays a dominant role for metallic states maintaining, as plotted in Fig. 4b. The absorption properties of free electrons ($(100)_{orth}$ oriented 2D $KNbO_3$ models) show a similar trend of confined states transition while the thickness variation (see ESI Fig. S6a†), although the ~4 nm (10 layers) model shows an anomalous absorption in the low-frequency range, which can be ascribe to the abrupt increase of the local DOS near E_F, as marked by pink arrow in ESI Fig. S6b.†

Conclusions

In summary, beyond well-known concepts for rearranging these surface electronic states (with extra electrons injecting) in 2D heterointerface or bare surface, our results show that additional holes injection can be maintained by the increase of surface polarity. The 2DEGs/2DHGs switching can be simply fulfilled by facet orientations. Distinct orientations change the polar discontinuity of alternating atom layers, corresponding to that huge surface energy differences. The thickness dependent behaviors of free electron/hole states subjecting to quantum confinement are addressed by the varied thickness of 2D

models. Compared with free electron states induced insulator–metal transition (4 nm sample still exists strong free electron states absorption), free hole states transition depends much stronger on the thickness of 2D quantum well, with a small critical value of ~2 nm. The formation of free electrons is more complex than free holes (contributed by O 2p states) due to the hybridization of s, p, d orbits in conduction bands. Such as one p band abnormally extends under E_F (among the split t_{2g} bands) for $(100)_{orth}$ oriented monolayer model at the extreme confined regime, acting to form an additional free electron conduction band (see ESI Fig. S5a†). Despite their differences, both of 2DEGs and 2DHGs are resulted from strong quantum confinement. Furthermore, the confined energy ($E - E_F$) and the total DOS occupying near E_F (which varies with sample thickness) jointly act on the metallic state transition, demonstrating that metallic states can be modulated not only by the amount of donor-like defects or adsorbates, but also simply by thickness variation.

In contrast to previous theoretical and experimental results,[3,4,24,26] our theoretical study reveals that the free holes can be obtained on high polar surface of perovskite oxides, gives the origins of oxides 2DEGs/2DHGs, including their intrinsic switching by surface polarity change and confined evolution behaviors with respect to quantum well thickness, emerging as a promising basis towards design the new generation all-oxides electronic devices.

Conflicts of interest

There are no conflicts to declare.

Acknowledgements

The work at HIT is supported by the Fundamental Research Funds for the Central Universities. Grant No. Hit. KISTP. 201401.

References

1 E. E. Mendez, L. Esaki and L. L. Chang, *Phys. Rev. Lett.*, 1985, **55**, 2216.
2 J. M. Kikkawa, *Science*, 1997, **277**, 1284–1287.
3 A. Ohtomo and H. Y. Hwang, *Nature*, 2004, **427**, 423–426.
4 W. Meevasana, P. D. C. King, R. H. He, S.-K. Mo, M. Hashimoto, A. Tamai, P. Songsiriritthigul, F. Baumberger and Z.-X. Shen, *Nat. Mater.*, 2011, **10**, 114–118.
5 A. F. Santander-Syro, O. Copie, T. Kondo, F. Fortuna, S. Pailhes, R. Weht, X. G. Qiu, F. Bertran, A. Nicolaou, A. Taleb-Ibrahimi, P. Le Fevre, G. Herranz, M. Bibes, N. Reyren, Y. Apertet, P. Lecoeur, A. Barthelemy and M. J. Rozenberg, *Nature*, 2011, **469**, 189–193.
6 C. Cen, S. Thiel, J. Mannhart and J. Levy, *Science*, 2009, **323**, 1026–1030.
7 S. Okamoto and A. J. Millis, *Nature*, 2004, **428**, 630–633.
8 C. Cen, S. Thiel, G. Hammerl, C. W. Schneider, K. E. Andersen, C. S. Hellberg, J. Mannhart and J. Levy, *Nat. Mater.*, 2008, **7**, 298–302.
9 N. Reyren, S. Thiel, A. D. Caviglia, L. F. Kourkoutis, G. Hammerl, C. Richter, C. W. Schneider, T. Kopp, A. S. Ruetschi, D. Jaccard, M. Gabay, D. A. Muller, J. M. Triscone and J. Mannhart, *Science*, 2007, **317**, 1196–1199.
10 A. Brinkman, M. Huijben, Z. M. Van, J. Huijben, U. Zeitler, J. C. Maan, V. D. W. Wg, G. Rijnders, D. H. Blank and H. Hilgenkamp, *Nat. Mater.*, 2007, **6**, 493–496.
11 S. Banerjee, O. Erten and M. Randeria, *Nat. Phys.*, 2013, **9**, 625–629.
12 A. F. Santander-Syro, F. Fortuna, C. Bareille, T. C. Rödel, G. Landolt, N. C. Plumb, J. H. Dil and M. Radović, *Nat. Mater.*, 2014, **13**, 1085.
13 N. C. Plumb, M. Salluzzo, E. Razzoli, M. Månsson, M. Falub, J. Krempasky, C. E. Matt, J. Chang, M. Schulte and J. Braun, *Phys. Rev. Lett.*, 2014, **113**, 086801.
14 M. Huijben, G. Rijnders, D. H. Blank, S. Bals, S. Van Aert, J. Verbeeck, G. Van Tendeloo, A. Brinkman and H. Hilgenkamp, *Nat. Mater.*, 2006, **5**, 556–560.
15 Y. Chen and N. Pryds, *Nat. Mater.*, 2018, **17**, 215–216.
16 H. Lee, N. Campbell, J. Lee, T. J. Asel, T. R. Paudel, H. Zhou, J. W. Lee, B. Noesges, J. Seo and B. Park, *Nat. Mater.*, 2018, **17**, 231–236.
17 W. Lu, J. Xiang, B. P. Timko, Y. Wu and C. M. Lieber, *Proc. Natl. Acad. Sci. U. S. A.*, 2005, **102**, 10046.
18 K. Nomura, J. Wunderlich, J. Sinova, B. Kaestner, A. H. MacDonald and T. Jungwirth, *Phys. Rev. B*, 2005, **72**, 245330.
19 R. Moriya, K. Sawano, Y. Hoshi, S. Masubuchi, Y. Shiraki, A. Wild, C. Neumann, G. Abstreiter, D. Bougeard and T. Koga, *Phys. Rev. Lett.*, 2014, **113**, 2916–2921.
20 M. D. Segall, P. J. D. Lindan, M. J. Probert, C. J. Pickard, P. J. Hasnip, S. J. Clark and M. C. Payne, *J. Phys.: Condens. Matter*, 2002, **14**, 2717.
21 J. P. Perdew, K. Burke and M. Ernzerhof, *Phys. Rev. Lett.*, 1996, **77**, 3865–3868.
22 Y. Bi, S. Ouyang, N. Umezawa, J. Cao and J. Ye, *J. Am. Chem. Soc.*, 2011, **133**, 6490–6492.
23 B. Silvi and A. Savin, *Nature*, 1994, **371**, 683–686.
24 P. Delugas, A. Filippetti, V. Fiorentini, D. I. Bilc, D. Fontaine and P. Ghosez, *Phys. Rev. Lett.*, 2011, **106**, 166807.
25 L. E. Brus, *J. Chem. Phys.*, 1984, **80**, 4403–4409.
26 Z. S. Popović, S. Satpathy and R. M. Martin, *Phys. Rev. Lett.*, 2008, **101**, 256801.

